

# Runtime optimization for vibrational structure on quantum computers: coordinates and measurement schemes

Marco Majland,<sup>1,2,3</sup> Rasmus Berg Jensen,<sup>2,3</sup> Mads Greisen Højlund,<sup>3</sup> Nikolaj Thomas Zinner,<sup>1,2</sup> and Ove Christiansen<sup>1,3</sup>

<sup>1</sup>*Kvantify Aps, DK-2300 Copenhagen S, Denmark*

<sup>2</sup>*Department of Physics and Astronomy, Aarhus University, DK-8000 Aarhus C, Denmark*

<sup>3</sup>*Department of Chemistry, Aarhus University, DK-8000 Aarhus C, Denmark*

One of the primary challenges prohibiting demonstrations of practical quantum advantages for near-term devices amounts to excessive measurement overheads for estimating relevant physical quantities such as ground state energies. However, with major differences between electronic and vibrational structure of molecules, the study of resource reductions for estimating anharmonic vibrational states remains relatively unexplored compared to its electronic counterpart. Importantly, bosonic commutation relations, distinguishable Hilbert spaces and vibrational coordinates allow different manipulations of the vibrational system in order to optimize the use of computational resources. In this work, we investigate the impact of different coordinate systems and measurement schemes on the runtime of estimating anharmonic vibrational states for a variety of three-mode (six-mode) molecules. We demonstrate an average of threefold (twofold), with up to sevenfold (fivefold), runtime reductions by employing appropriate coordinate transformations. Despite such reductions, crude estimates of runtimes for chemically motivated Ansätze and realistic potential energy surfaces are very considerable and thus further improvements are necessary to demonstrate practical quantum advantages.

## I. INTRODUCTION

The simulation of many-body quantum systems on quantum computers is a promising candidate to achieve computational advantages in both academic and practical applications [1–4]. However, current quantum devices are subject to noise and error, restricting the available computational resources. While practical quantum advantages are yet to be demonstrated, hybrid quantum-classical algorithms such as the variational quantum eigensolver are expected to provide such demonstrations [5–9]. The electronic structure problem on quantum computers has been significantly investigated in recent years while the vibrational structure problem remains relatively unexplored [10–13]. Importantly, research suggests that classically intractable vibrational structure problems may be solved on quantum computers prior to electronic equivalents [10]. Estimating eigenstates of many-body Hamiltonians using the variational quantum eigensolver requires sampling expectation values of Pauli operators with a trial state. However, it has empirically been shown that the estimation of the electronic ground state for small molecules to chemical accuracy requires infeasible runtimes due to sampling overhead, denoted as the measurement problem [14, 15]. Different measurement schemes have been employed to reduce the sampling overhead, including grouping Pauli products into mutually commuting sets [16–25], classical shadow tomography [26–29], low-rank factorizations of the electronic Hamiltonian [30] and algebraic approaches [31]. However, current studies have been investigating electronic Hamiltonians only and thus measurement schemes for vibrational structure remains unexplored [14]. In contrast to the two-body electronic Hamiltonian, the many-body vibrational Hamiltonian

contains up to  $N$ -body coupling terms between the vibrational modes and depends on the choice of vibrational coordinates. Different coordinate systems impact the vibrational interactions and may be exploited to obtain approximate mode decoupling. Such a decoupling modifies the interaction patterns between modes, affecting the distribution of small and large terms, which has been observed to imply that many higher mode terms become less important, though not vanishing. This can be seen as better decoupling of coordinates and fewer very important terms, but as all terms are effected, this does not necessarily imply optimal variances. In this paper, we investigate the impact of different measurement schemes and coordinate systems for ground state estimation of a variety of three- and six-mode molecules. With the ground state calculation runtime depending on the variance of the Hamiltonian, we demonstrate an average of threefold (twofold), with up to sevenfold (fivefold), reduction in total runtime using appropriate coordinate transformations. Although such reductions shorten the route to practical quantum advantage, we show crude estimates of total runtimes for a single energy calculation of up to several hours where a classical computation would require only seconds. Thus, research should focus on developing measurement schemes and improved hardware-efficient Ansätze adapted to the vibrational Hamiltonian.

## II. BACKGROUND

### A. Sampling expectation values

Consider a qubit Hamiltonian  $H = \sum_i h_i P_i$  where  $h_i$  denotes matrix elements and

$$P_i = \bigotimes_j \sigma_j^\alpha, \quad \alpha \in \{x, y, z\}, \quad (1)$$

denotes a product of Pauli operators. In the variational quantum eigensolver, the ground state energy functional is estimated as the expectation value of the Hamiltonian with a trial state  $|\psi(\boldsymbol{\theta})\rangle$ ,

$$E(\boldsymbol{\theta}) = \langle \psi(\boldsymbol{\theta}) | H | \psi(\boldsymbol{\theta}) \rangle = \sum_i h_i \langle \psi(\boldsymbol{\theta}) | P_i | \psi(\boldsymbol{\theta}) \rangle. \quad (2)$$

To reduce the number of measurements, the Hamiltonian may be grouped into mutually commuting sets

$$S = \{H_\alpha = \sum_\beta H_\alpha^\beta \mid [H_\alpha^\beta, H_\alpha^\gamma] = 0\} \quad (3)$$

such that  $H = \sum_\alpha H_\alpha$ . Each set,  $H_\alpha$ , may be rotated into a diagonal basis and measured simultaneously. Let  $m_\alpha$  denote the number of measurements per group and  $\mathcal{M} = \sum_\alpha m_\alpha$  the total number of measurements. By optimizing  $\{m_\alpha\}$  the number of measurements required for a given precision  $\epsilon$  reads

$$\mathcal{M} = \left( \frac{\sum_\alpha \sqrt{\text{var}(H_\alpha)}}{\epsilon} \right)^2 \quad (4)$$

if  $m_i$  are optimally allocated for each group [18]. With the total number of measurements depending on the variance of each group, the measurements may be optimized by optimizing the total group variances.

### B. Measurement schemes

The qubit-space measurement schemes group mutually commuting Pauli products into measurable sets according to either qubit-wise commutativity (QWC) or full commutativity (FC) [16–18, 20, 21, 24, 32]. In the QWC scheme, the Pauli products commute locally for each qubit subspace, whereas the FC scheme only requires commutativity of the full tensor products. The advantage of the QWC scheme is that it requires only one-qubit rotations whereas the FC scheme requires both one- and two-qubit gates to diagonalize the operators. By transforming a set of fully commuting operators into a set of qubit-wise commuting operators, the diagonalization block may be implemented using  $\mathcal{O}(N_q^2 / \log(N_q))$  two-qubit gates where  $N_q$  denotes the number of qubits. In the case of electronic Hamiltonians, QWC schemes were numerically demonstrated to be inferior to FC schemes even when accounting

for the increased circuit depths [18, 19]. One of the most widely used measurement schemes amounts to the sorted insertion (SI) algorithm [18, 22]. The SI algorithm orders the Pauli operators according to the absolute value of the matrix elements. The groups of mutually commuting operators are generated by initially choosing the operator with largest matrix element, looping through the list of operators and extracting operators which commute with the initial operator. The groups may be generated based on both QWC and FC schemes. Despite its relatively simple greedy sorting algorithm, the SI algorithm was demonstrated to outperform recent classical shadow tomographic methods [18]. Thus, the SI algorithm will be used in this work.

## III. VIBRATIONAL STRUCTURE

### A. Vibrational Hamiltonian and potential energy surfaces

Consider a molecule with  $M$  vibrational modes described by a set of mass-weighted normal coordinates (or other orthogonal coordinates)  $q_m$ . Neglecting the Coriolis and pseudopotential terms of the Watson operator [33, 34], the vibrational Hamiltonian reads

$$H = -\frac{1}{2} \sum_{m=1}^M \frac{\partial^2}{\partial q_m^2} + \sum_{m=1}^M V(q_m) + \sum_{m < m'}^M V(q_m, q_{m'}) + \dots \quad (5)$$

where the potential in principle contains terms coupling up to  $M$  modes simultaneously. The potential energy surface (PES), i.e. the vibrational potential, may be obtained using a variety of methods, e.g. using Taylor expansion or the adaptive density-guided approach (ADGA) [35]. A Taylor expansion of the PESs around the equilibrium geometry provides the PESs in an economical form but suffers from the limited reliability of such expansions including limited radius of convergence and high risk of providing a variationally unbound potential. In contrast, the ADGA is a robust and accurate black-box procedure, which builds the potential according to the need as determined from the vibrational calculation. The ADGA uses densities of the vibrational wavefunction to iteratively sample the surface in a physically motivated way. After generating the PESs, the vibrational Hamiltonian may be transformed into a qubit Hamiltonian using existing encoding algorithms [11–13].

#### 1. Vibrational coordinates

A standard choice of coordinates is normal coordinates which provide excellent first order insights into the vibrations of stiff molecules close to their equilibrium structures. The benefit of normal coordinates for stiff molecules close to their equilibrium structures is that they decouple the

Hamiltonian to second order. However, the use of normal coordinates does not suppress higher-order terms (in fact, the contrary might be true away from equilibrium). This motivates the search for other types of coordinates that ensure some degree of decoupling of the Hamiltonian. Such coordinates include various kinds of curvilinear coordinates (e.g. bond angles and lengths or polyspherical coordinates), which are often deemed chemically relevant. These coordinates typically reduce the couplings in the potential energy at the price of increasing the coupling level and overall complexity of the kinetic energy. To avoid this latter complication, we focus on rectilinear coordinates that are derived from normal coordinates by orthogonal transformations. This includes optimized coordinates [36, 37] obtained by minimizing the vibrational self-consistent field energy for a given PES and localized coordinates [38] obtained by applying some localization scheme to a set of normal coordinates. A pragmatic and inexpensive compromise is offered by the so-called hybrid optimized and localized coordinates [39], which minimize a cost function including an energy term and a localization term,

$$f(\mathbf{q}) = w_E E(\mathbf{q}) + w_L L(\mathbf{q}). \quad (6)$$

The energy is taken to be the vibrational self-consistent field energy on a second-order PES. We will refer to the localization weight  $w_L$  as the coordinate localization parameter. Setting  $w_L = 0$  yields normal coordinates, while large  $w_L$  yield very localized (but not necessarily meaningful) coordinates. We emphasize the fact that, as was mentioned in the introduction, approximate decoupling of the Hamiltonian does not necessarily provide optimal variances.

## 2. Distinguishability of vibrational modes

Since the vibrational modes are distinguishable (in contrast to electrons), the vibrational Hilbert space factorizes into distinguishable one-mode subspaces. As a result, these subspace factorizations allow for further flexibility in measuring general operators (products of one-mode operators) since non-overlapping operators commute. For example, consider two operators for a five-mode molecule,  $A_0 \otimes A_1 \otimes \mathbb{1} \otimes \mathbb{1} \otimes \mathbb{1} \in H^{(0,1)}$  and  $\mathbb{1} \otimes \mathbb{1} \otimes A_2 \otimes A_3 \otimes A_4 \in H^{(2,3,4)}$ , where  $H^{\mathbf{m}}$  is the set of operators acting non-trivially only on the set of modes  $\mathbf{m}$ . Such sets are referred to as mode combinations and the set of all mode combinations,  $\mathfrak{M} = \{\mathbf{m}\}$ , is called the mode combination range (MCR). As the two example operators above do not overlap, they commute and may be measured simultaneously. Thus, grouping the operators according to their overlaps reduce the total number of groups to be measured. To obtain such groupings, the vibrational Hamiltonian may be reformulated using mode combinations. For example, for a three-mode system  $\mathfrak{M} = \{(0), (1), (2), (0, 1), (0, 2), (1, 2), (1, 2, 3)\}$ . Using

mode combinations, the vibrational Hamiltonian may be re-written as

$$H = \sum_{\mathbf{m} \in \mathfrak{M}} H^{\mathbf{m}}. \quad (7)$$

Note that these effects are implicitly included in the SI algorithm since the commutativity based on mode combinations is also contained in the QWC and FC schemes. However, to study the direct effect of vibrational mode distinguishability, mode combinations may be exploited to obtain mutually commuting groups of products of one-mode operators. The operators within an mode combination do not mutually commute and must be diagonalized. Non-overlapping mode combinations are therefore combined and the SI algorithm used to decompose these sets into mutually commuting groups. Depending on whether the QWC/FC scheme is used to determine mutually commuting groups, the algorithms which group depending on the MCR are denoted QWC(FC)/MCR. As an example, the MCR grouping for five-mode systems is presented in Appendix B. In contrast to the SI algorithm, which groups entirely based on the coefficients of the Hamiltonian, grouping based on MCRs first will in general yield different groups than plain SI. Additionally, the MCR grouping allows for trivial parallelization of the following sorted insertions.

## B. Runtime estimation

The runtime of calculating vibrational ground state energies depends on the preparation time for the qubits and quantum gates, circuit runtime, qubit readout time, time of classical processing and the reset times of qubits/quantum gates. Assuming that the primary contribution arises from the circuit runtime, the following runtime model is used in the estimations

$$t = \mathcal{M} T_{\text{circuit}}, \quad (8)$$

where  $\mathcal{M}$  is the number of measurements and  $T_{\text{circuit}}$  is the circuit runtime [14]. In order to estimate  $T_{\text{circuit}}$ , we consider the unitary vibrational coupled cluster with singles and doubles (UVCCSD) Ansatz [12, 13], the vibrational equivalent of unitary coupled cluster with singles and doubles [5]. The UVCCSD state is defined as

$$|\psi(\boldsymbol{\theta})\rangle = e^{T(\boldsymbol{\theta}) - T^\dagger(\boldsymbol{\theta})} |\Phi\rangle \quad (9)$$

with the cluster operator  $T = T_1 + T_2$  given by

$$T_1 = \sum_m \sum_{a^m} \theta_{a^m}^m a_a^{m\dagger} a_i^m \quad (10)$$

and

$$T_2 = \sum_{m < m'} \sum_{a^m b^{m'}} \theta_{a^m b^{m'}}^{mm'} a_a^{m\dagger} a_i^m a_b^{m'\dagger} a_i^{m'}. \quad (11)$$

The cluster amplitudes are real parameters while the operators  $a_a^{m\dagger}$  and  $a_i^m$  create and annihilate occupation in the one-mode basis functions. The vibrational operators are mapped to a qubit representation and compiled to a set of quantum gates. The Ansatz compilation may be performed using the strategies presented in Ref. 5 involving the CNOT ladder and Trotterization. Using the conventional CNOT ladder to implement the Trotterized wavefunction, the primary contribution for the total circuit runtime arises from the CNOT gates of the double excitations. In a direct mapping, an arbitrary double excitation operator transforms such that

$$\begin{aligned} a_i^\dagger a_j a_m^\dagger a_n - \text{h. c.} &= \sigma_i^+ \sigma_j^- \sigma_m^+ \sigma_n^- - \text{h. c.} \\ &= 2i(\sigma_i^x \sigma_j^y \sigma_m^x \sigma_n^x + \sigma_i^y \sigma_j^x \sigma_m^x \sigma_n^x \\ &\quad + \sigma_i^y \sigma_j^y \sigma_m^x \sigma_n^y + \sigma_i^x \sigma_j^y \sigma_m^y \sigma_n^x \\ &\quad + \sigma_i^x \sigma_j^x \sigma_m^x \sigma_n^y + \sigma_i^x \sigma_j^x \sigma_m^y \sigma_n^x \\ &\quad + \sigma_i^x \sigma_j^y \sigma_m^y \sigma_n^y + \sigma_i^y \sigma_j^x \sigma_m^y \sigma_n^y) \end{aligned} \quad (12)$$

where each term may be diagonalized using six CNOT gates such that the total number of CNOT gates for the implementation of a double excitation amounts to 48. This transformation rule is general, and not restricted to the vibrational second quantized operators of Eqs. (9) to (11), hence the notation  $a_i^\dagger$ ,  $a_j$ , etc. Assuming a fixed number of virtual basis functions  $n$  for each mode, the UVCCSD Ansatz contains  $\binom{M}{2}n^2$  double excitations. The total number of CNOT gates required to implement the double excitations of the UVCCSD Ansatz is thus  $48\binom{M}{2}n^2$ . If the time to perform a single CNOT gate is  $T_{\text{CNOT}} = 1.0 \mu\text{s}$ , the circuit runtime becomes

$$T_{\text{UVCCSD}} = 48 \left( \frac{\sum_\alpha \sqrt{\text{var}(H_\alpha)}}{\epsilon} \right)^2 T_{\text{CNOT}} \binom{M}{2} n^2. \quad (13)$$

To minimize the runtime in the case of electronic structure, a large variety of Ansätze have been developed with significantly reduced circuit depths which were shown to reach chemical accuracy for small molecules [5]. While some progress has been made in the development of such Ansätze for vibrational structure, the hardware-efficient Ansatz presented in Ref. 13 does not achieve sufficient accuracy and convergence even for small vibrational systems. Note that the runtimes may be further reduced by estimating the energy expectation values using near-term approximations of quantum phase estimation [40].

#### IV. COMPUTATIONAL DETAILS

A total of 18 molecules were considered, including nine triatomic (three-mode) systems and nine tetratomic (six-mode) systems. All electronic structure calculations were performed at the CCSD(F12\*)(T)/cc-pVDZ-F12 level [41, 42] of theory as implemented in the Turbomole [43] program suite. The geometry of each molecule

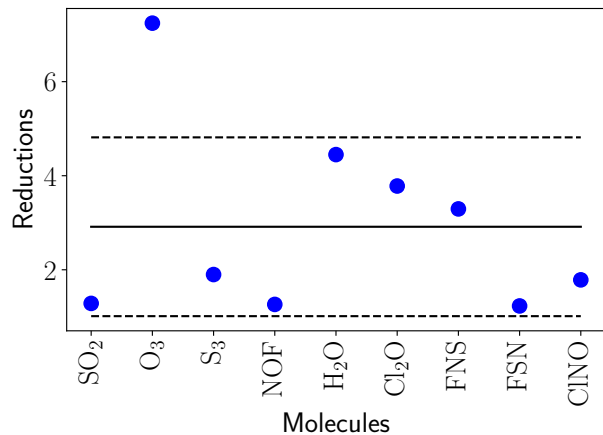


FIG. 1. Reductions of the three-mode molecules which are calculated as the ratio between the minimum and maximum variances for all coordinate systems excluding the localization parameter  $w_i = 1.0 \times 10^{-3}$  since these coordinates were inferior for all molecules.

was optimized using numerical gradients, after which a numerical Hessian was computed and used to generate normal coordinates and hybrid optimized and localized coordinates with a series of localization parameters,  $w_l$ . Coordinate generation was performed using the MidasCpp program [44], which was also used to construct electronic PESs with the ADGA algorithm for each coordinate set. Following the PES construction, vibrational self-consistent field calculations were carried out in large B-spline bases. The few lowest vibrational self-consistent field modals (four for the three-mode systems, two for the six-mode systems) were then used as a basis for representing the Hamiltonian in a second quantized format and for performing conventional full vibrational configuration interaction calculations. The representation of the Hamiltonian in a suitable format is fully automatized in MidasCpp (see Appendix A for a few considerations in this regard). The Hamiltonian and the full vibrational configuration interaction wavefunction were finally transformed to a qubit representation and the variance computed using a locally developed Python3 code. For each molecule and coordinate system, the measurement groups are generated using the SI algorithm with the QWC and FC schemes. These algorithms were described in Sections II B and III A 2.

#### V. RESULTS

To estimate the impact of coordinate transformations, the ratio of the lowest and highest variance for each molecule is calculated. This yields a number we will refer to as the reduction. In these calculations, all molecules were shown to exhibit the largest variances for strongly localized coordinates with localization parameter  $w_l = 1.0 \times 10^{-3}$ . Such behaviour is not surprising,

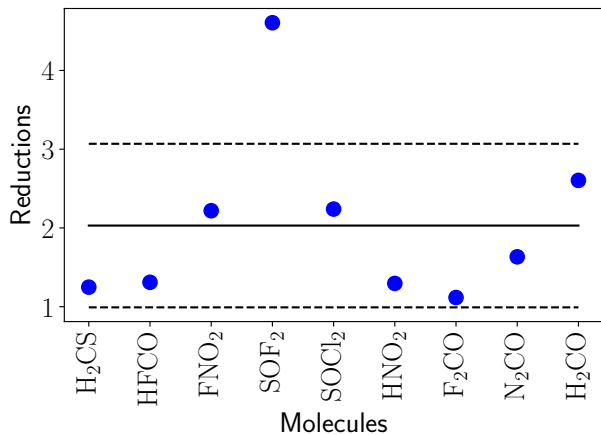


FIG. 2. Reductions of the six-mode molecules which are calculated as the ratio between the minimum and maximum variances for all coordinate systems excluding the localization parameter  $w_L = 1.0 \times 10^{-3}$  since these coordinates were inferior for all molecules.

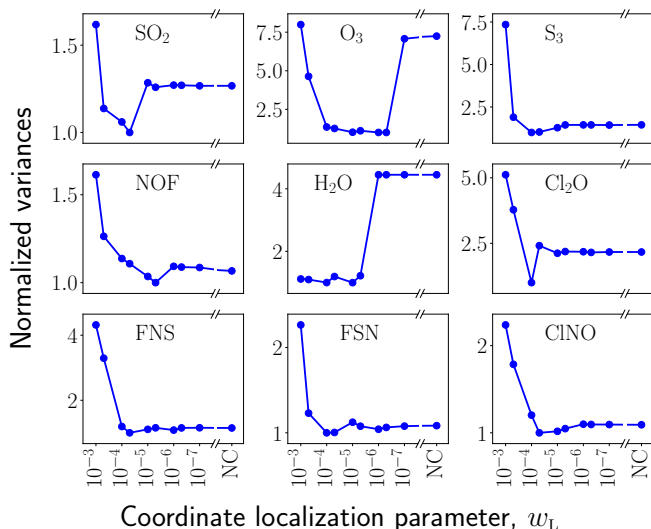


FIG. 3. Variances of the three-mode molecules normalized relative to the minimum variance for all coordinate systems. For each coordinate system, the variance depicted amounts to the optimal variance considering both the QWC and FC schemes. Each hybrid optimized and localized coordinate system is represented by its localization parameter  $w_L$  and normal coordinate refers to normal coordinates.

since strongly localized coordinates are not necessarily physically meaningful, and thus these results were omitted from the reduction calculations. These reductions are depicted in Figs. 1 and 2. The minimum variances generated by the grouping algorithms for each coordinate system are depicted in Figs. 3 and 4. Several conclusions based hereupon may be drawn in terms of coordinate transformations.

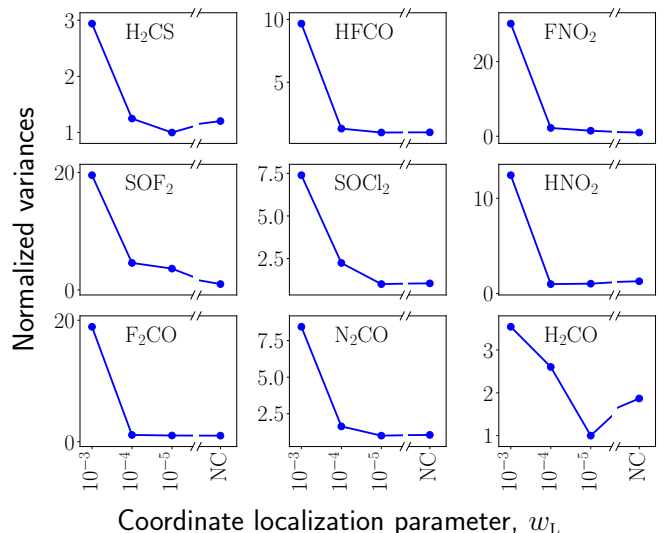


FIG. 4. Variances of the three-mode molecules normalized relative to the minimum variance for all coordinate systems. For each coordinate system, the variance depicted amounts to the optimal variance considering both the QWC and FC schemes. Each hybrid optimized and localized coordinate system is represented by its localization parameter  $w_L$ .

### A. Molecular symmetry

We see no clear pattern relating to point group symmetry as exemplified by the molecules  $O_3$  and  $S_3$ . Despite being extremely similar with respect to symmetry and structure, they behave quite differently with respect to the computed variances (see Figs. 1, 3 and 5). These results highlights the complexity of the interdependence between the the choice of coordinates, the details of the PES and the vibrational structure of the molecule.

### B. QWC and FC schemes

To study the QWC and FC schemes, the variances were calculated for each measurement scheme which is depicted in Figs. 5 and 6. In contrast to the electronic structure, QWC and FC schemes do not exhibit any clear tendencies in terms of systematically lowering the variances. With the differences being close to negligible, the FC schemes appear to be less favourable compared to the QWC schemes due to increased circuit depths of the former. The vibrational operators are very different from their electronic counterparts. Since the Hilbert spaces differ in structure, with the electronic Hilbert space being expanded in spin-orbitals and the vibrational Hilbert space being expanded in modal basis functions, the variability of modal basis dimensions impact the QWC/FC commutation relations between the vibrational operators. These differences may contribute to the different performances of the QWC and FC schemes compared to their

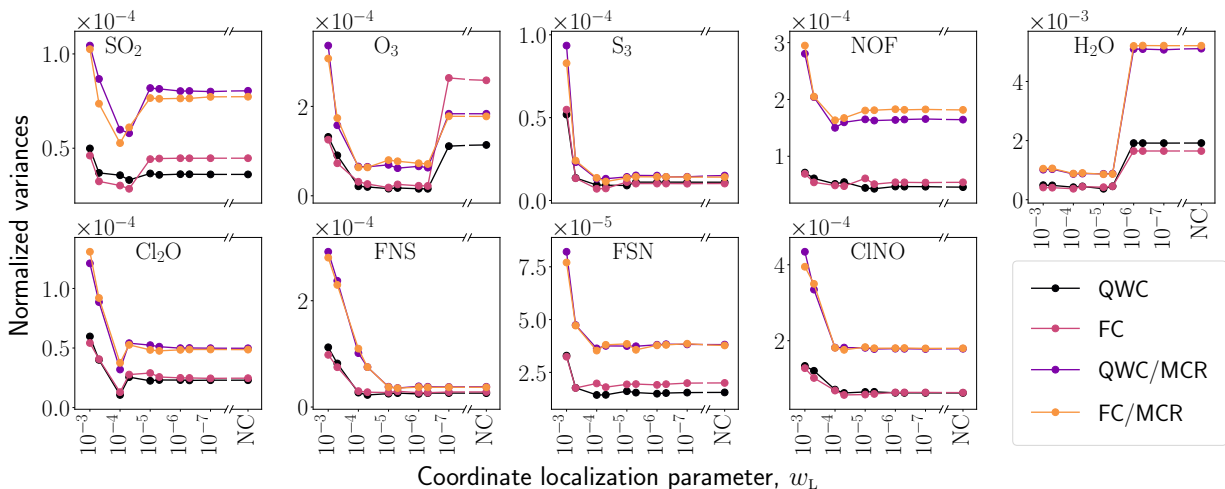


FIG. 5. Variances of the three-mode molecules for each grouping scheme (Sections II B and III A 2). The hybrid optimized and localized coordinate coordinate systems are defined by their localization parameter  $w_L$ , with normal coordinate denoting normal coordinates. All grouping schemes employ sorted insertion with the commutator schemes indicated in the legend. In general sorted insertion produces the smallest variances and the discrepancy between commutativity schemes is small.

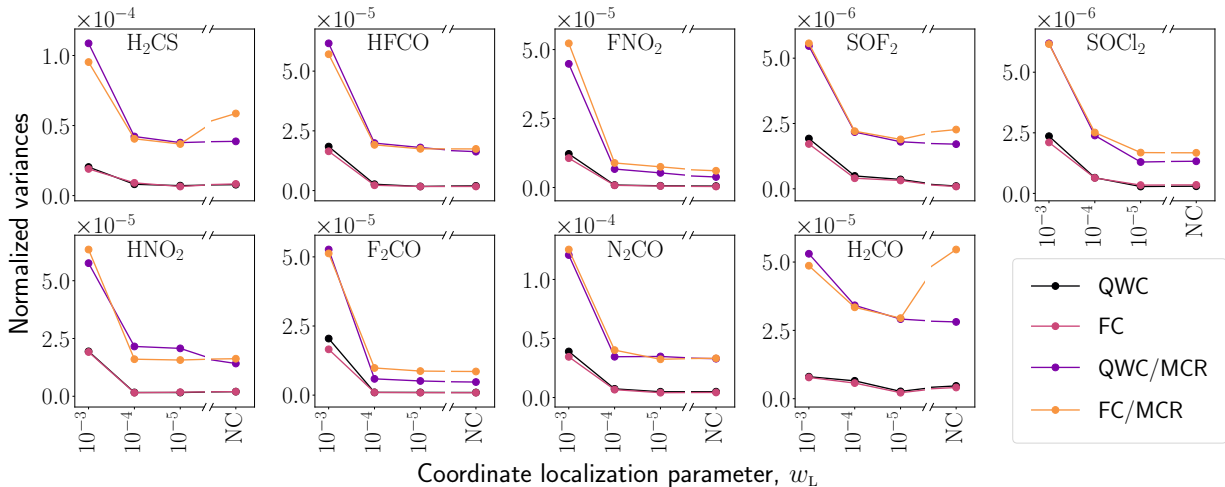


FIG. 6. Variances of the six-mode molecules for each grouping scheme (Sections II B and III A 2). The hybrid optimized and localized coordinate coordinate systems are defined by their localization parameter  $w_L$ , with normal coordinate denoting normal coordinates. All grouping schemes employ sorted insertion with the commutator schemes indicated in the legend. In general sorted insertion produces the smallest variances and the discrepancy between commutativity schemes is minuscule.

electronic structure counterparts. Such differences are seen in Figs. 5 and 6, where the three-mode molecules are described by four modals per mode whereas the six-mode molecules are described by two modals per mode. In the first case, some differences between QWC/FC appear, whereas in the second case the QWC/FC perform identically.

### C. Invariance and reductions

The mean reduction for the three-mode (six-mode) molecules is around 3 (2) with relatively large deviations. The largest improvements for the three-mode (six-mode)

molecules amounts to around a fivefold (sevenfold) reduction. Meanwhile, some of the molecules were shown to exhibit approximate invariance under reasonable coordinate transformations.

### D. Vibrational heuristics

From Figs. 5 and 6 it is clear that plain SI outperforms the methods based on MCR. SI thus seems to be the best option, which in some sense is not surprising. The MCR methods essentially divide the set of all Hamiltonian terms into smaller subsets, in a chemically motivated fashion. The SI algorithm then sorts these subsets in

order to obtain the final groups, such that the sorting is restricted, meaning that the sorting has less flexibility. For larger molecules this might however be an advantage if the sorting overhead becomes significant due to the non-linear scaling of sorting algorithms. This scaling implies that in general sorting of multiple small sets is faster than the sorting of one large set. Additionally, the sorting of smaller sets is trivially parallelizable in contrast with plain SI. As seen for  $S_3$  and FNS the MCR methods has the potential to yield groupings of comparable variance to plain SI hence it is possible that the MCR methods might yield a faster overall time to solution for large molecules. For the three-mode systems the vast majority of terms are contained within the mode combination  $\mathbf{m} = (1, 2, 3)$ , hence the potential speed-up in group generation is negligible here. However, for larger molecules, the amount of combinations of higher-order terms increase rapidly.

### E. Runtime estimates

Using the estimates of Eq. (2) and the minimum variances for each molecule, the runtimes for estimating a single energy evaluation are shown in Table I. Even with the optimal choice of coordinates, the runtimes are considerable for the UVCCSD Ansatz. We note that the runtime estimates are significantly larger for the three-mode systems than for the six-mode systems, which is rather counterintuitive. In both cases, the Hilbert space has dimension  $D = N^M = 46$  (where  $N$  is the number of modals per mode) but the number and distribution of Hamiltonian terms differs. For a three-mode coupled Hamiltonian, the number of second quantized terms (in the format of Appendix A) is

$$N_{\text{terms}} = \binom{M}{3}N^6 + \binom{M}{2}N^4 + \binom{M}{1}N^2 \quad (14)$$

$$= \begin{cases} 4912 & \text{for } M = 3, N = 4, \\ 1544 & \text{for } M = 6, N = 2. \end{cases} \quad (15)$$

These numbers alone do not explain the difference in runtime, but it should be recalled that the three-mode systems are dominated by a single three-mode coupling with many terms while the six-mode systems have a comparatively large number of mode couplings that each contribute a relatively small number of terms. This impacts the grouping of terms after the qubit transformation and, in turn, the variances and runtimes.

## VI. CONCLUSION

In this work, we have presented different vibrational coordinates that provide reductions in runtime for quantum computations of anharmonic vibrational wavefunctions using realistic potential energy surfaces (PESs). It was

shown that an average of threefold (twofold), with up to sevenfold (fivefold), reductions may be achieved by appropriately transforming the vibrational coordinates for three-mode (six-mode) molecules. One must emphasize the size of the molecules which were used in the benchmarks. Localized coordinates are generally favourable for relatively large molecules for which delocalized interactions may be negligible. Thus, localized coordinates should be further investigated in the context of larger systems to investigate the performance for larger molecules. Furthermore, it was demonstrated that the qubit-wise commutativity (QWC) scheme may provide similar variance reductions as compared to the full commutativity (FC) scheme, contrary to what has been demonstrated for electronic structure. Thus, the FC schemes appear to be less favourable compared to the QWC schemes due to increased circuit depths. Such differences between electronic and vibrational structure may arise due to the different commutations relations (fermionic/bosonic). Additionally, the Hilbert spaces differ in structure, with the electronic Hilbert space being expanded in spin-orbitals and the vibrational Hilbert space being expanded in modal basis functions. Combining the sorted insertion (SI) algorithm with grouping non-overlapping interaction terms does not provide more optimal groupings compared to the SI algorithm. They do however have the potential for faster group generation of large molecules, where this overhead may become important. These results agree with previous conclusions for electronic structure where minimizing the total number of groups does not necessarily provide optimal variances. Despite the reductions obtained by performing optimal coordinate transformations, the crude unitary vibrational coupled cluster with singles and doubles (UVCCSD) estimates indicate considerable runtimes for estimating ground states, requiring further research to focus on methods for reduction of resources in order to provide practical quantum advantages in vibrational structure.

## VII. ACKNOWLEDGEMENTS

O.C. acknowledges support from the Independent Research Fund Denmark through grant number 1026-00122B. The authors acknowledge funding from the Novo Nordisk Foundation through grant NNF20OC0065479. PES calculations were performed at the Centre for Scientific Computing Aarhus (CSCAA).

## VIII. DATA AVAILABILITY

The code related to the study is available upon reasonable request to the authors.

3 mode molecules	S <sub>3</sub>	FSN	FNS	Cl <sub>2</sub> O	SO <sub>2</sub>	O <sub>3</sub>	NOF	CINO	H <sub>2</sub> O
Runtime (min)	43.79	135.63	136.29	144.15	202.45	243.78	627.28	675.37	3308.35
6 mode molecules	SOCl <sub>2</sub>	SOF <sub>2</sub>	FNO <sub>2</sub>	F <sub>2</sub> CO	HNO <sub>2</sub>	HF <sub>2</sub> CO	H <sub>2</sub> CO	N <sub>2</sub> CO	H <sub>2</sub> CS
Runtime (min)	8.04	9.08	29.10	41.03	75.26	83.70	141.47	155.40	176.71

TABLE I. Runtime estimates of the sets of three-mode and six-mode benchmark molecules. The three-mode bases includes 4 modals per mode, whereas the six-mode bases only include 2 modals per mode, which is the reason that the six-mode runtime estimates are shorter than those of the three-mode molecules.

### Appendix A: Operator format

The PES for the vibrational problem is usually represented in a sum-of-products (SOP) form,

$$H = \sum_t c_t \prod_{m \in \mathbf{m}_t} h^{m,t} = \sum_{\mathbf{m}} H^{\mathbf{m}}, \quad (\text{A1})$$

where  $c_t$  is the coefficient for the term indexed by  $t$ . Any given term includes a product of one-mode operators  $h^{m,t}$  for a set of modes  $\mathbf{m}_t$ . The one-mode operators can be written as

$$h^{m,t} = \sum_{p^m q^m} h_{p^m q^m}^{m,t} a_p^{m\dagger} a_q^m. \quad (\text{A2})$$

The SOP format covers most practically relevant cases such as Taylor expanded potentials and more elaborate polynomial representations such as those generated by the adaptive density-guided approach (ADGA) algorithm [35]. When designing algorithms for classical computers, it is extremely beneficial to keep the operator in the SOP form and never expand the products of one-mode operators. However, for the purpose of transforming the Hamiltonian into qubit format, we expand all product into simple strings of creating and annihilation operators. As a simple example, consider the terms pertaining to a given two-mode combination,

$$\begin{aligned} H^{mn} &= \sum_t c_t h^{m,t} h^{n,t} \\ &= \sum_{p^m q^m} \sum_{p^n q^n} \sum_t c_t h_{p^m q^m}^{m,t} h_{p^n q^n}^{n,t} a_p^{m\dagger} a_q^m a_p^{n\dagger} a_q^n \\ &\equiv \sum_{p^m q^m} \sum_{p^n q^n} H_{(p^m q^m)(p^n q^n)}^{m,n} a_p^{m\dagger} a_q^m a_p^{n\dagger} a_q^n. \end{aligned} \quad (\text{A3})$$

This example is readily generalized to terms containing more modes. A trivial but important point is that the

number of coefficients in Eq. (A3) does not depend on the number of terms in the SOP expansion in Eq. (A1).

### Appendix B: mode combination range (MCR) grouping for five-mode systems

For a five-mode system with one-, two-, and three-mode couplings in the Hamiltonian, the grouping based on MCR may be obtained by grouping disjoint two- and three-body couplings along with one-body couplings. The two- and three-body couplings yield  $\{H^{(i,j,k)} + H^{(m,n)} | (m,n) \notin (i,j,k)\}$  while the one-body couplings yield  $\{H^{(i)}\}$ . An example is presented in the following:

- $S_0 = \{H^{(0,1,2)}, H^{(3,4)}\}$
- $S_1 = \{H^{(1,2,3)}, H^{(0,4)}\}$
- $S_2 = \{H^{(2,3,4)}, H^{(0,1)}\}$
- $S_3 = \{H^{(0,2,3)}, H^{(1,4)}\}$
- $S_4 = \{H^{(0,3,4)}, H^{(1,2)}\}$
- $S_5 = \{H^{(0,1,4)}, H^{(2,3)}\}$
- $S_6 = \{H^{(1,3,4)}, H^{(0,2)}\}$
- $S_7 = \{H^{(0,1,3)}, H^{(2,4)}\}$
- $S_8 = \{H^{(0,2,4)}, H^{(1,3)}\}$
- $S_9 = \{H^{(0)}, H^{(1)}, H^{(2)}, H^{(3)}, H^{(4)}\}$

The terms commute since their mode couplings are disjoint. The terms also exhibit maximal mode coupling since all modes are active in the terms. However, the operators for each mode coupling within an MCR do not mutually commute and must be diagonalized. Using the SI algorithm, each MCR group may be decomposed into subgroups which mutually commute. The MCR grouping for the three- and six-mode molecules studied in this work are generated analogously for the five-mode system. Due to the more complex combinations for the six-mode system, however, we present the example of a five-mode system for simplicity.



- [1] A. J. Daley, I. Bloch, C. Kokail, S. Flannigan, N. Pearson, M. Troyer, and P. Zoller, “Practical quantum advantage in quantum simulation,” *Nature*, vol. 607, pp. 667–676, July 2022. Number: 7920 Publisher: Nature Publishing Group.
- [2] S. Lee, J. Lee, H. Zhai, Y. Tong, A. M. Dalzell, A. Kumar, P. Helms, J. Gray, Z.-H. Cui, W. Liu, M. Kastoryano, R. Babbush, J. Preskill, D. R. Reichman, E. T. Campbell, E. F. Valeev, L. Lin, and G. K.-L. Chan, “Is there evidence for exponential quantum advantage in quantum chemistry?,” Aug. 2022. arXiv:2208.02199 [physics, physics:quant-ph].
- [3] V. E. Elfving, B. W. Broer, M. Webber, J. Gavartin, M. D. Halls, K. P. Lorton, and A. Bochevarov, “How will quantum computers provide an industrially relevant computational advantage in quantum chemistry?,” Sept. 2020. arXiv:2009.12472 [physics, physics:quant-ph].
- [4] A. Aspuru-Guzik, A. D. Dutoi, P. J. Love, and M. Head-Gordon, “Simulated quantum computation of molecular energies,” *Science (New York, N.Y.)*, vol. 309, pp. 1704–1707, Sept. 2005.
- [5] A. Anand, P. Schleich, S. Alperin-Lea, P. W. K. Jensen, S. Sim, M. Díaz-Tinoco, J. S. Kottmann, M. Degroote, A. F. Izmaylov, and A. Aspuru-Guzik, “A Quantum Computing View on Unitary Coupled Cluster Theory,” *Chemical Society Reviews*, vol. 51, no. 5, pp. 1659–1684, 2022. arXiv:2109.15176 [physics, physics:quant-ph].
- [6] R. Babbush, D. W. Berry, I. D. Kivlichan, A. Y. Wei, P. J. Love, and A. Aspuru-Guzik, “Exponentially more precise quantum simulation of fermions in second quantization,” *New Journal of Physics*, vol. 18, p. 033032, Mar. 2016. Publisher: IOP Publishing.
- [7] R. Babbush, D. W. Berry, Y. R. Sanders, I. D. Kivlichan, A. Scherer, A. Y. Wei, P. J. Love, and A. Aspuru-Guzik, “Exponentially more precise quantum simulation of fermions in the configuration interaction representation,” *Quantum Science and Technology*, vol. 3, p. 015006, Dec. 2017. Publisher: IOP Publishing.
- [8] J. R. McClean, J. Romero, R. Babbush, and A. Aspuru-Guzik, “The theory of variational hybrid quantum-classical algorithms,” *New Journal of Physics*, vol. 18, p. 023023, Feb. 2016. Publisher: IOP Publishing.
- [9] “A variational eigenvalue solver on a photonic quantum processor | Nature Communications.”
- [10] N. P. D. Sawaya, F. Paesani, and D. P. Tabor, “Near- and long-term quantum algorithmic approaches for vibrational spectroscopy,” *Physical Review A*, vol. 104, p. 062419, Dec. 2021. Publisher: American Physical Society.
- [11] N. P. D. Sawaya, T. Menke, T. H. Kyaw, S. Johri, A. Aspuru-Guzik, and G. G. Guerreschi, “Resource-efficient digital quantum simulation of d-level systems for photonic, vibrational, and spin-s Hamiltonians,” *npj Quantum Information*, vol. 6, pp. 1–13, June 2020. Number: 1 Publisher: Nature Publishing Group.
- [12] S. McArdle, A. Mayorov, X. Shan, S. Benjamin, and X. Yuan, “Digital quantum simulation of molecular vibrations,” *Chemical Science*, vol. 10, no. 22, pp. 5725–5735, 2019. arXiv:1811.04069 [quant-ph].
- [13] P. J. Ollitrault, A. Baiardi, M. Reiher, and I. Tavernelli, “Hardware Efficient Quantum Algorithms for Vibrational Structure Calculations,” *Chemical Science*, vol. 11, no. 26, pp. 6842–6855, 2020. arXiv:2003.12578 [quant-ph].
- [14] J. F. Gonthier, M. D. Radin, C. Buda, E. J. Daskocil, C. M. Abuan, and J. Romero, “Identifying challenges towards practical quantum advantage through resource estimation: the measurement roadblock in the variational quantum eigensolver,” Tech. Rep. arXiv:2012.04001, arXiv, Dec. 2020. arXiv:2012.04001 [quant-ph] type: article.
- [15] G. Wang, D. E. Koh, P. D. Johnson, and Y. Cao, “Minimizing estimation runtime on noisy quantum computers,” *PRX Quantum*, vol. 2, p. 010346, Mar. 2021. arXiv:2006.09350 [quant-ph].
- [16] A. Zhao, A. Tranter, W. M. Kirby, S. F. Ung, A. Miyake, and P. Love, “Measurement reduction in variational quantum algorithms,” *Physical Review A*, vol. 101, p. 062322, June 2020. arXiv:1908.08067 [quant-ph].
- [17] V. Verteletskyi, T.-C. Yen, and A. F. Izmaylov, “Measurement Optimization in the Variational Quantum Eigensolver Using a Minimum Clique Cover,” *The Journal of Chemical Physics*, vol. 152, p. 124114, Mar. 2020. arXiv:1907.03358 [physics, physics:quant-ph].
- [18] T.-C. Yen, A. Ganeshram, and A. F. Izmaylov, “Deterministic improvements of quantum measurements with grouping of compatible operators, non-local transformations, and covariance estimates,” Apr. 2022. arXiv:2201.01471 [physics, physics:quant-ph].
- [19] Z. P. Bansingh, T.-C. Yen, P. D. Johnson, and A. F. Izmaylov, “Fidelity overhead for non-local measurements in variational quantum algorithms,” May 2022. arXiv:2205.07113 [physics, physics:quant-ph].
- [20] T.-C. Yen, V. Verteletskyi, and A. F. Izmaylov, “Measuring all compatible operators in one series of a single-qubit measurements using unitary transformations,” Tech. Rep. arXiv:1907.09386, arXiv, Mar. 2020. arXiv:1907.09386 [physics, physics:quant-ph] type: article.
- [21] I. Hamamura and T. Imamichi, “Efficient evaluation of quantum observables using entangled measurements,” *npj Quantum Information*, vol. 6, pp. 1–8, June 2020. Number: 1 Publisher: Nature Publishing Group.
- [22] O. Crawford, B. v. Straaten, D. Wang, T. Parks, E. Campbell, and S. Brierley, “Efficient quantum measurement of Pauli operators in the presence of finite sampling error,” *Quantum*, vol. 5, p. 385, Jan. 2021. Publisher: Verein zur Förderung des Open Access Publizierens in den Quantenwissenschaften.
- [23] S. Choi, T.-C. Yen, and A. F. Izmaylov, “Improving quantum measurements by introducing “ghost” Pauli products,” Aug. 2022. arXiv:2208.06563 [physics, physics:quant-ph].
- [24] A. F. Izmaylov, T.-C. Yen, and I. G. Ryabinkin, “Revising the measurement process in the variational quantum eigensolver: is it possible to reduce the number of separately measured operators?,” *Chemical Science*, vol. 10, pp. 3746–3755, Mar. 2019. Publisher: The Royal Society of Chemistry.
- [25] A. F. Izmaylov, T.-C. Yen, R. A. Lang, and V. Verteletskyi, “Unitary partitioning approach to the measurement problem in the Variational Quantum Eigensolver method,” Tech. Rep. arXiv:1907.09040, arXiv, Oct. 2019. arXiv:1907.09040 [physics, physics:quant-ph] type: article.

- [26] C. Hadfield, S. Bravyi, R. Raymond, and A. Mezzacapo, "Measurements of Quantum Hamiltonians with Locally-Biased Classical Shadows," June 2020. arXiv:2006.15788 [quant-ph].
- [27] H.-Y. Huang, R. Kueng, and J. Preskill, "Efficient Estimation of Pauli Observables by Derandomization," *Physical Review Letters*, vol. 127, p. 030503, July 2021. Publisher: American Physical Society.
- [28] C. Hadfield, "Adaptive Pauli Shadows for Energy Estimation," May 2021. arXiv:2105.12207 [quant-ph].
- [29] B. Wu, J. Sun, Q. Huang, and X. Yuan, "Overlapped grouping measurement: A unified framework for measuring quantum states," May 2021. arXiv:2105.13091 [quant-ph].
- [30] W. J. Huggins, J. McClean, N. Rubin, Z. Jiang, N. Wiebe, K. B. Whaley, and R. Babbush, "Efficient and Noise Resilient Measurements for Quantum Chemistry on Near-Term Quantum Computers," *npj Quantum Information*, vol. 7, p. 23, Dec. 2021. arXiv:1907.13117 [physics, physics:quant-ph].
- [31] T.-C. Yen and A. F. Izmaylov, "Cartan Subalgebra Approach to Efficient Measurements of Quantum Observables," *PRX Quantum*, vol. 2, p. 040320, Oct. 2021. Publisher: American Physical Society.
- [32] A. Jena, S. Genin, and M. Mosca, "Pauli Partitioning with Respect to Gate Sets," July 2019. arXiv:1907.07859 [quant-ph].
- [33] J. K. Watson, "Simplification of the molecular vibration-rotation hamiltonian," *Molecular Physics*, vol. 15, pp. 479–490, Jan. 1968.
- [34] J. K. Watson, "The vibration-rotation hamiltonian of linear molecules," *Molecular Physics*, vol. 19, pp. 465–487, Oct. 1970.
- [35] M. Sparta, D. Toffoli, and O. Christiansen, "An adaptive density-guided approach for the generation of potential energy surfaces of polyatomic molecules," *Theoretical Chemistry Accounts*, vol. 123, pp. 413–429, Aug. 2009.
- [36] K. Yagi, M. Keçeli, and S. Hirata, "Optimized coordinates for anharmonic vibrational structure theories," *The Journal of Chemical Physics*, vol. 137, p. 204118, Nov. 2012. Publisher: American Institute of Physics.
- [37] B. Thomsen, K. Yagi, and O. Christiansen, "Optimized coordinates in vibrational coupled cluster calculations," *The Journal of Chemical Physics*, vol. 140, p. 154102, Apr. 2014. Publisher: American Institute of Physics.
- [38] C. R. Jacob and M. Reiher, "Localizing normal modes in large molecules," *The Journal of Chemical Physics*, vol. 130, p. 084106, Feb. 2009.
- [39] E. L. Klinting, C. König, and O. Christiansen, "Hybrid Optimized and Localized Vibrational Coordinates," *The Journal of Physical Chemistry A*, vol. 119, pp. 11007–11021, Nov. 2015. Publisher: American Chemical Society.
- [40] P. D. Johnson, A. A. Kunitsa, J. F. Gonthier, M. D. Radin, C. Buda, E. J. Doskocil, C. M. Abuan, and J. Romero, "Reducing the cost of energy estimation in the variational quantum eigensolver algorithm with robust amplitude estimation," Mar. 2022. arXiv:2203.07275 [physics, physics:quant-ph].
- [41] C. Hättig, D. P. Tew, and A. Köhn, "Communications: Accurate and efficient approximations to explicitly correlated coupled-cluster singles and doubles, CCSD-F12," *The Journal of Chemical Physics*, vol. 132, p. 231102, June 2010.
- [42] K. A. Peterson, T. B. Adler, and H.-J. Werner, "Systematically convergent basis sets for explicitly correlated wavefunctions: The atoms H, He, B–Ne, and Al–Ar," *The Journal of Chemical Physics*, vol. 128, p. 084102, Feb. 2008.
- [43] "Turbomole V7.5." TURBOMOLE GmbH.
- [44] D. G. Artiukhin, O. Christiansen, I. H. Godtlielsen, E. M. Gras, W. Györffy, M. B. Hansen, M. B. Hansen, E. L. Klinting, J. Kongsted, C. König, D. Madsen, N. K. Madsen, K. Monrad, G. Schmitz, P. Seidler, K. Sneskov, M. Sparta, B. Thomsen, D. Toffoli, and A. Zocante, "MidasCpp," 2020.